Online Supplemental Appendix to Optimal Nonparametric Range-Based Volatility Estimation

Tim Bollerslev* Jia Li† Qiyuan Li‡

October 9, 2023

Abstract

This supplemental appendix is divided into three sections. In Section SA, we introduce optimal estimators for spot quarticity and precision. Section SB provides additional empirical findings, including results for the Dollar/Yen exchange rate, volatility estimates derived from multiple candlesticks, and comparisons among alternative estimators. Section SC presents the results of a simulation study, demonstrating the robustness of the proposed estimators when implemented using 5-minute frequency candlestick observations in the presence of microstructure noise.

*Department of Economics, Duke University, Durham, NC 27708; e-mail: boller@duke.edu.

†School of Economics, Singapore Management University, Singapore; e-mail: jiali@smu.edu.sg.

‡School of Economics, Singapore Management University, Singapore; e-mail: qyli.2019@phdecons.smu.edu.sg.

SA Optimal Estimation for Quarticity and Precision

SA.1 AMRE Estimators for Quarticity and Precision

In Theorem S1 and Theorem S2, we provide closed-form expressions for the AMRE estimators of the spot quarticity, denoted as σ_t^4, and the spot precision, denoted as σ_t^{-1}, respectively. However, due to a technical integrability issue, we have only derived the closed-form solution for the AMRE spot precision estimator under Stein's loss.

Theorem S1. *Under the same setting as Theorem 1, the AMRE range-based estimator for the spot quarticity σ_t^4 under Stein's loss is asymptotically unbiased and is given by*

$$\hat{\sigma}^4_{\text{Stein}} \equiv \frac{128 w_i^4}{15} \cdot \frac{G_0(a_i/w_i) - H_0(|r_i|/w_i)}{G_4(a_i/w_i) - H_4(|r_i|/w_i)},$$

while the AMRE range-based estimator for σ_t^4 under standardized quadratic loss equals

$$\hat{\sigma}^4_{\text{Quad}} \equiv 256 w_i^4 \cdot \frac{G_4(a_i/w_i) - H_4(|r_i|/w_i)}{G_8(a_i/w_i) - H_8(|r_i|/w_i)}.$$

Theorem S2. *Under the same setting as Theorem 1, the AMRE range-based estimator for the spot precision σ_t^{-1} under Stein's loss is asymptotically unbiased and is given by*

$$\hat{\sigma}^{-1}_{\text{Stein}} \equiv \sqrt{\frac{\pi}{2}} w_i^{-1} \cdot \frac{G_0(a_i/w_i) - H_0(|r_i|/w_i)}{G_{-1}(a_i/w_i) - H_{-1}(|r_i|/w_i)},$$

where $G_0(\cdot)$ and $H_0(\cdot)$ are defined in (2.10) and (2.11) in the main text and

$$\begin{aligned} G_{-1}(x) &\equiv x\Big(\psi_0\Big(\frac{1-x}{2}\Big) - \psi_0\Big(\frac{1+x}{2}\Big)\Big) + \frac{1-x^2}{4}\Big(\psi_1\Big(\frac{1-x}{2}\Big) + \psi_1\Big(\frac{1+x}{2}\Big)\Big), \\ H_{-1}(x) &\equiv x\Big(\psi_0\Big(1-\frac{x}{2}\Big) - \psi_0\Big(\frac{x}{2}\Big)\Big) - \frac{x^2}{4}\Big(\psi_1\Big(1-\frac{x}{2}\Big) + \psi_1\Big(\frac{x}{2}\Big)\Big). \end{aligned}$$

In parallel to Tables 1 and 2 for the spot variance and spot volatility estimators in the main text, Tables S1 and S2 below display the asymptotic bias, variance, and relative efficiency of various estimators for spot quarticity and precision, respectively. The results are qualitatively similar to the ones presented in the main text.

We once again observe that Stein-AMRE estimators demonstrate lower asymptotic risk compared to shape-constrained estimators, not only under Stein's loss but also under the quadratic loss. Interestingly, the relative efficiencies of shape-constrained estimators are considerably lower when estimating quarticity and precision as opposed to volatility estimation. For instance, the relative efficiency of $(\hat{\sigma}_{\text{BLUE}})^4$ as a spot quarticity estimator is a mere 25.5% under the quadratic loss function. These risk comparisons further emphasize the efficiency advantages of employing AMRE estimators for a wider variety of volatility estimation tasks.

Table S1: Asymptotic Risk Properties of Alternative Estimators for Spot Quarticity

			Relative Efficiency	
Estimator	Bias	Variance	Stein	Quadratic
$\hat{\sigma}^4_{\text{Stein}}$	0.000	1.305	1.000	0.544
$\hat{\sigma}^4_{\text{Quad}}$	-0.564	0.392	0.535	1.000
$(\hat{\sigma}^2_{\text{GK}})^2$	0.271	2.206	0.921	0.312
$(\hat{\sigma}_{\text{BLUE}})^4$	0.423	2.608	0.874	0.255

Note: The table reports the asymptotic biases, variances, and relative efficiency under Stein's and quadratic risks for each of the regular estimators indicated in the first column.

Table S2: Asymptotic Risk Properties of Alternative Estimators for Spot Precision

			Relative Efficiency	
Estimator	Bias	Variance	Stein	Quadratic
$\hat{\sigma}^{-1}_{\text{Stein}}$	0.000	0.066	1.000	1.000
$(\hat{\sigma}^2_{\text{GK}})^{-1/2}$	0.099	0.081	0.838	0.725
$\hat{\sigma}^{-1}_{\text{BLUE}}$	0.065	0.076	0.912	0.825

Note: The table reports the asymptotic biases, variances, and relative efficiency under Stein's and quadratic risks for each of the regular estimators indicated in the first column. Since the quadratic-AMRE estimator is unavailable, the relative efficiencies of the spot precision estimators are calculated with respect to the Stein-AMRE estimator under both Stein's loss and the quadratic loss.

SA.2 Proofs

PROOF OF THEOREM S1. The proof is similar to that of Theorem 2 in the main text, and so, we only emphasize the main difference. Recall the definition of (ξ_1, ξ_2, ξ_3) from Lemma A2 in the main text. The minimum-risk scale-equivariant estimation function for volatility under the limit problem is given by

$$w_i^4 \cdot \frac{1}{\mathbb{E}[\xi_1^4 | \xi_2 = a_1/w_i, \xi_3 = |r_i|/w_i]} \quad \text{and} \quad w_i^4 \cdot \frac{\mathbb{E}[\xi_1^4 | \xi_2 = a_1/w_i, \xi_3 = |r_i|/w_i]}{\mathbb{E}[\xi_1^8 | \xi_2 = a_1/w_i, \xi_3 = |r_i|/w_i]},$$

for Stein's loss and quadratic loss, respectively. The asserted closed-form expressions are obtained by applying Lemma A2 with $q = 4$ and 8. *Q.E.D.*

PROOF OF THEOREM S2. Under Stein's loss, the minimum-risk scale-equivariant estimation function for the precision in the limit problem is given by $w_i^{-1}/\mathbb{E}[\xi_1^{-1} | \xi_2 = a_1/w_i, \xi_3 = |r_i|/w_i]$. The remaining task is to derive its closed-form expression, which requires a more refined argument than those used in the analysis for optimal variance and/or volatility estimation.

Let $g_\xi(\cdot)$ denote the joint density of (ξ_1, ξ_2, ξ_3). Note that

$$\mathbb{E}[\xi_1^{-1} | \xi_2 = y, \xi_3 = z] = \frac{\int_0^\infty x^{-1} g_\xi(x, y, z) dx}{\int_0^\infty g_\xi(x, y, z) dx}, \tag{SA.1}$$

and the denominator $\int_0^\infty g_\xi(x, y, z) dx = G_0(y) - H_0(z)$ as implied by Lemma A2. It remains to compute $\int_0^\infty x^{-1} g_\xi(x, y, z) dx$. Recall that $g_\xi(x, y, z) = 4\sqrt{2/\pi} \sum_{k=-\infty}^{\infty} \big(C_k(x, z) - D_k(x, y)\big)$, where

$$\begin{aligned} C_k(x, z) &\equiv k^2 x^2 \big((2k + z)^2 x^2 - 1\big) \exp\Big(-\frac{(2k + z)^2 x^2}{2}\Big), \\ D_k(x, y) &\equiv k(1 + k) x^2 \big((2k + 1 - y)^2 x^2 - 1\big) \exp\Big(-\frac{(2k + 1 - y)^2 x^2}{2}\Big). \end{aligned}$$

By a direct integration, we have

$$\begin{aligned} \int_0^\infty x^{-1} C_k(x, z) dx &= \frac{k^2}{(2k + z)^2}, \\ \int_0^\infty x^{-1} D_k(x, y) dx &= \frac{k(k + 1)}{(2k + 1 - y)^2}. \end{aligned}$$

Therefore, the numerator in (SA.1) can be rewritten as

$$\begin{aligned} & 4\sqrt{\frac{\pi}{2}} \int_0^\infty x^{-1} \sum_{k=-\infty}^{\infty} \big(C_k(x, z) - D_k(x, y)\big) dx \\ &= 4\sqrt{\frac{\pi}{2}} \sum_{k=-\infty}^{\infty} \Big(\frac{k^2}{(2k + z)^2} - \frac{k(k + 1)}{(2k + 1 - y)^2}\Big) \\ &= \sqrt{\frac{\pi}{2}} \sum_{k=0}^{\infty} \Big(\frac{k^2}{(k + \frac{z}{2})^2} + \frac{(k + 1)^2}{(k + 1 - \frac{z}{2})^2} - \frac{k(k + 1)}{(k + \frac{1-y}{2})^2} - \frac{k(k + 1)}{(k + \frac{1+y}{2})^2}\Big). \end{aligned} \tag{SA.2}$$

By (5.7.6) and (5.15.1) in Olver et al. (2010), we have

$$\psi_0(z_1) - \psi_0(z_2) = \sum_{k=0}^{\infty}\Big(\frac{1}{z_2+k} - \frac{1}{z_1+k}\Big), \tag{SA.3}$$

$$\psi_1(z_1) + \psi_1(z_2) = \sum_{k=0}^{\infty}\bigg(\frac{1}{(z_1+k)^2} + \frac{1}{(z_2+k)^2}\bigg). \tag{SA.4}$$

Note that, the summand in (SA.2) may be rewritten as

$$\begin{aligned}
&\frac{k^2}{(k+\frac{z}{2})^2} + \frac{(k+1)^2}{(k+1-\frac{z}{2})^2} - \frac{k(k+1)}{(k+\frac{1-y}{2})^2} - \frac{k(k+1)}{(k+\frac{1+y}{2})^2} \\
&= y\bigg(\frac{1}{\frac{1+y}{2}+k} - \frac{1}{\frac{1-y}{2}+k}\bigg) + \frac{1}{4}\cdot(1-y^2)\bigg(\frac{1}{(\frac{1+y}{2}+k)^2} + \frac{1}{(\frac{1-y}{2}+k)^2}\bigg) \\
&\quad - z\bigg(\frac{1}{\frac{z}{2}+k} - \frac{1}{1-\frac{z}{2}+k}\bigg) + \frac{1}{4}\cdot z^2\bigg(\frac{1}{(\frac{z}{2}+k)^2} + \frac{1}{(1-\frac{z}{2}+k)^2}\bigg).
\end{aligned} \tag{SA.5}$$

Combining (SA.2)–(SA.5) yields

$$4\sqrt{\frac{\pi}{2}}\int_0^{\infty} x^{-1}\sum_{k=-\infty}^{\infty}\big(C_k(x,z) - D_k(x,y)\big)dx = \sqrt{\frac{\pi}{2}}\big(G_{-1}(y) - H_{-1}(z)\big).$$

This completes the derivation of the closed-form expression for (SA.1). Since that function is continuous almost everywhere (recall that polygamma functions are meromorphic), the estimator is indeed regular, and so, defines the AMRE estimator under the original nonparametric model as asserted in Theorem S2. *Q.E.D.*

SB Additional Empirical Results

SB.1 Comparisons of Single Versus Multiple Candlestick Estimators

The spot volatility estimates for the VOO ETF plotted in Figure **??** in the main text are formed using the single-candlestick estimator $\hat{\sigma}_{\text{Stein}}$ described in Theorem **??**. To illustrate the practical use of the AMRE k-candlestick estimators detailed in Section **??**, we also compute the AMRE spot volatility estimator $\hat{\sigma}_{\text{Stein}}(k)$ for $k = 2$. Figure S1 visually compares the single-candlestick estimates with the two-candlestick estimates.

Unsurprisingly, the two-candlestick estimates essentially manifest as "averages" of the corresponding pair of single-candlestick estimates. As discussed in more detail in the main text, such aggregation is suitable when the underlying volatility does not change "too much," but it can be problematic when volatility moves rapidly. This, of course, is exactly what happens after many FOMC announcements, as highlighted, for example, by the November 2, 2022 announcement.

Figure S2 presents similar results for the Dollar/Yen exchange rate. The comparisons between the single and two-candlestick estimators evidence the same general features as the comparisons of the $k = 1$ and $k = 2$ estimates for the VOO ETF in Figure S1. Meanwhile, comparing the estimates across Figure S1 and Figure S2, there are also notable differences between the way in which the spot volatility of the VOO ETF and the Dollar/Yen exchange rate vary around the time of the FOMC announcements, reflecting the differential response of the equity and currency markets to monetary policy shocks.

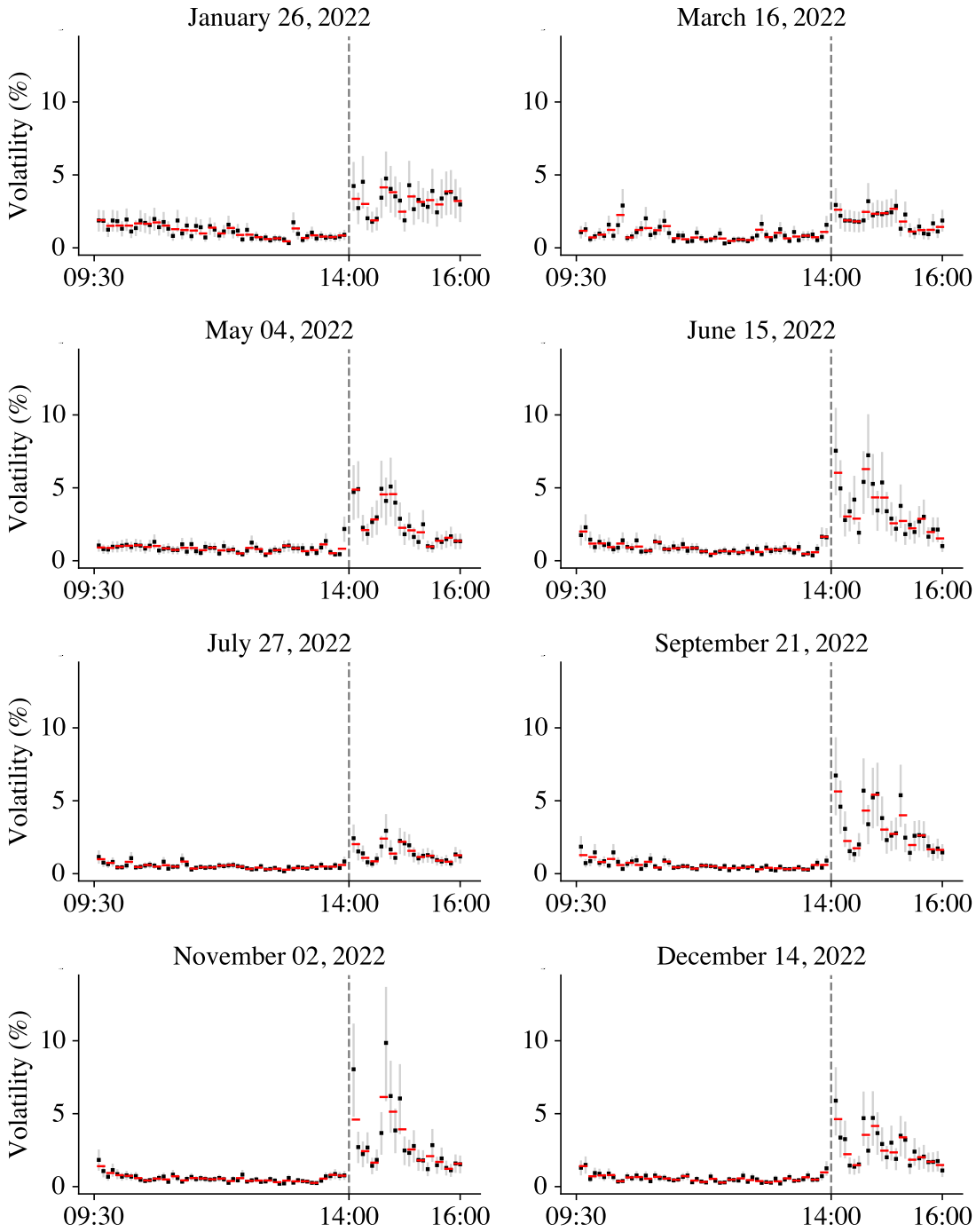

Figure S1: **Comparison of Single-Candlestick and Two-Candlestick Estimates.** The figure plots the estimates of the AMRE spot volatility estimator $\hat{\sigma}_{\text{Stein}}$ constructed using one candlestick (dot) and two candlesticks (dash), expressed in daily percentage terms and calculated using individual 5-minute frequency candlesticks of the VOO ETF. Pointwise confidence intervals at the 90% level for the single-candlestick estimates are also plotted.

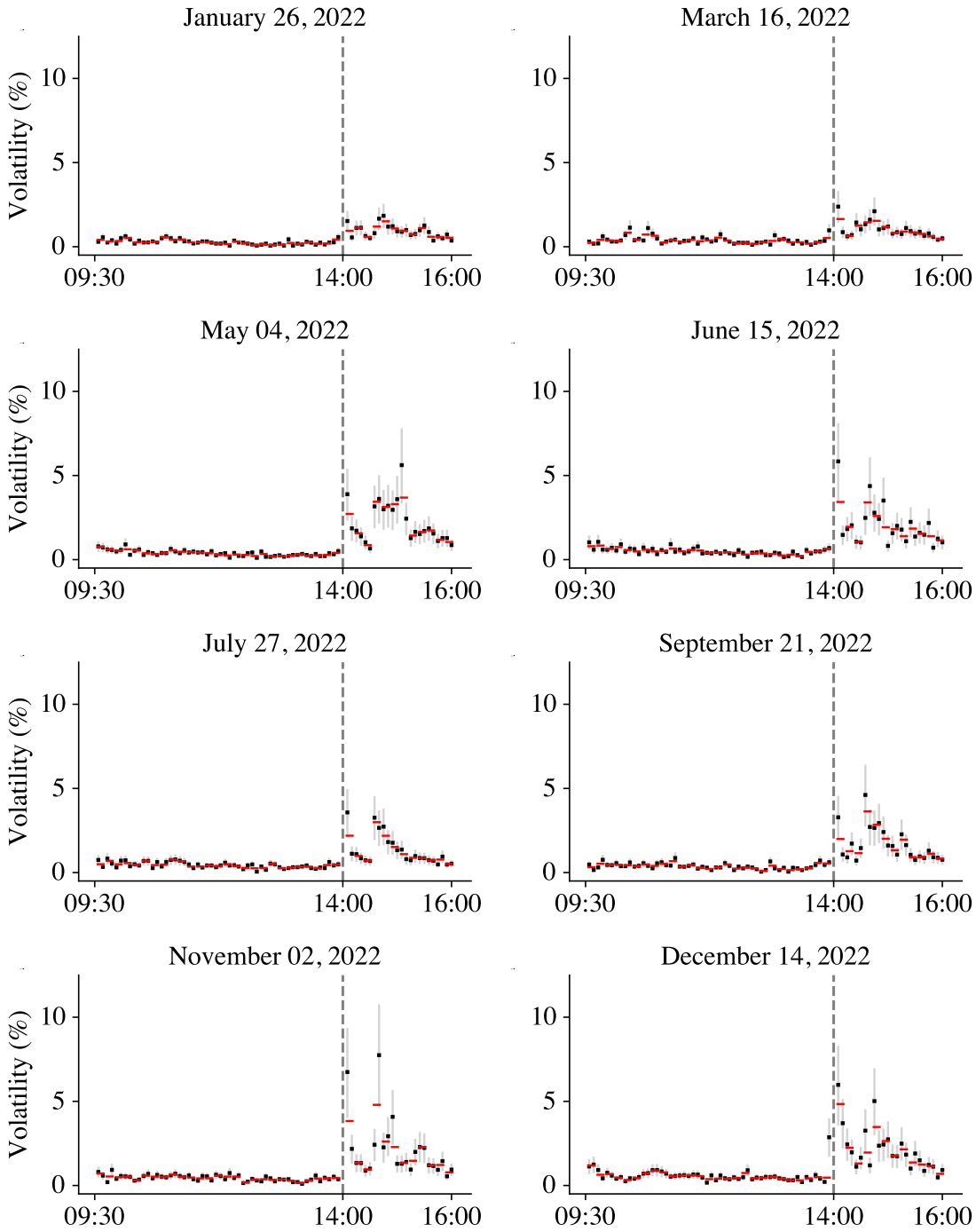

Figure S2: **Comparison of Single-Candlestick and Two-Candlestick Estimates.** The figure plots the estimates of the AMRE spot volatility estimator $\hat{\sigma}_{\text{Stein}}$ constructed using one candlestick (dot) and two candlesticks (dash), expressed in daily percentage terms and calculated using individual 5-minute frequency candlesticks of the Dollar/Yen exchange rate. Pointwise confidence intervals at the 90% level for the single-candlestick estimates are also plotted.

SB.2 Comparison Among Alternative Estimators

The empirical estimates in the main text, as well as those in Section SB.1 above, are based on AMRE estimators for the spot volatility σ_t derived under Stein's loss. The use of alternative estimators would yield different estimates. It is helpful to understand the magnitude of these differences.

To this end, we report summary statistics for the relative discrepancy between alternative estimators of σ_t^p for $p \in \{1, 2, 4\}$. For each σ_t^p, we consider four estimators: the AMRE estimators $\hat{\sigma}^p_{\text{Stein}}$ and $\hat{\sigma}^p_{\text{Quad}}$, a transformed version of the Garman–Klass variance estimator $(\hat{\sigma}^2_{\text{GK}})^{p/2}$, and a transformed version of Li et al.'s (2022) volatility estimator $(\hat{\sigma}_{\text{BLUE}})^p$. Table S3 presents the results for alternative single-candlestick estimators with respect to the AMRE estimator $\hat{\sigma}^p_{\text{Stein}}$ (Panel A) or $\hat{\sigma}^p_{\text{Quad}}$ (Panel B). Specifically, when comparing $(\hat{\sigma}^2_{\text{GK}})^{p/2}$ with $\hat{\sigma}^p_{\text{Stein}}$ in Panel A, we calculate the relative discrepancy measure as

$$\sqrt{\text{sample average of } \left| \frac{(\hat{\sigma}^2_{\text{GK}})^{p/2} - \hat{\sigma}^p_{\text{Stein}}}{\hat{\sigma}^p_{\text{Stein}}} \right|^2},$$

where the sample average is computed across all spot estimates for the eight FOMC announcement days in 2022. We do the calculations separately for the VOO ETF and the Dollar/Yen exchange rate. Similar results for estimators based on two candlesticks are reported in Table S4.

The main findings may be summarized as follows. Firstly, we note that alternative estimates for σ_t^p exhibit larger differences when p is larger. For example, for volatility estimation (i.e., $p = 1$), the linear $\hat{\sigma}_{\text{BLUE}}$ estimator differs from the Stein-AMRE estimator $\hat{\sigma}_{\text{Stein}}$ by 2.5% and 4.4% for the VOO ETF and the Dollar/Yen, respectively. The corresponding relative discrepancy measures increase to 8.1% and 12.2% for variance estimation (i.e., $p = 2$), and further increase to 44.5% and 53.7% for quarticity estimation (i.e., $p = 4$).

Secondly, comparing the discrepancy numbers between Panel A and Panel B shows that the shape-constrained estimators, $(\hat{\sigma}^2_{\text{GK}})^{p/2}$ and $(\hat{\sigma}_{\text{BLUE}})^p$, are more distinct from $\hat{\sigma}^p_{\text{Quad}}$ than $\hat{\sigma}^p_{\text{Stein}}$. This is also consistent with Figures 2 and 3 in the main text, which show the alternative estimation functions. This suggests that under the quadratic loss criterion, suboptimal estimators can be quite different from the AMRE estimator. For example, $\hat{\sigma}_{\text{BLUE}}$ differs from $\hat{\sigma}_{\text{Quad}}$ by 6.6% (resp. 8.1%) for VOO (resp. Dollar/Yen), while the relative differences increase to more than 30% for variance estimation. For the more extreme case of estimating quarticity σ_t^4, the AMRE estimator $\hat{\sigma}^4_{\text{Quad}}$ is generally much smaller (due to shrinkage) than any of the other estimators, as evidenced by the large discrepancy measures seen in the $p = 4$ columns in Panel B.

Finally, we observe that the relative discrepancies between alternative estimators are generally

larger in the two-candlestick case than the single-candlestick case. As a case in point, the $\hat{\sigma}_{\text{BLUE}}$ and $\hat{\sigma}_{\text{Stein}}$ volatility estimators based on a single-candlestick display a high degree of similarity, with discrepancy summary statistics of 2.5% for the VOO and 4.4% for the Dollar/Yen, respectively, while the two-candlestick versions exhibit more significant differences, with discrepancy summary statistics equal to 4.6% for the VOO and 12.1% for the Dollar/Yen.

In summary, the comparisons in Tables S3 and S4 highlight potentially large empirical differences among the different estimators. The extent of the discrepancy depends, among other factors, on the estimand (i.e., σ_t^p), the loss function employed in deriving the AMRE estimator, and the number of candlesticks utilized in the estimation. It is, of course, also data dependent, as evidenced by the differences in the summary statistics for the VOO ETF and the Dollar/Yen exchange rate for the same set of estimators and times.

Table S3: Relative Discrepancies for Alternative One-Candlestick Estimators

	VOO			Dollar/Yen		
	$p=1$	$p=2$	$p=4$	$p=1$	$p=2$	$p=4$
Panel A: Comparison versus the Stein-AMRE Estimator						
$\hat{\sigma}^p_{\text{Quad}}$	0.058	0.210	0.587	0.057	0.211	0.593
$(\hat{\sigma}^2_{\text{GK}})^{p/2}$	0.059	0.094	0.361	0.089	0.142	0.389
$(\hat{\sigma}_{\text{BLUE}})^p$	0.025	0.081	0.445	0.044	0.122	0.537
Panel B: Comparison versus the Quadratic-AMRE Estimator						
$\hat{\sigma}^p_{\text{Stein}}$	0.062	0.268	1.480	0.061	0.270	1.561
$(\hat{\sigma}^2_{\text{GK}})^{p/2}$	0.056	0.297	2.145	0.074	0.399	2.216
$(\hat{\sigma}_{\text{BLUE}})^p$	0.066	0.347	2.558	0.081	0.379	3.032

Note: The table reports summary statistics for the relative differences of alternative single-candlestick estimators of σ^p_t with respect to the AMRE estimators. In Panel A and Panel B, the benchmark AMRE estimators are set as $\hat{\sigma}^p_{\text{Stein}}$ and $\hat{\sigma}^p_{\text{Quad}}$, respectively. The reported values are the root mean squared relative differences, calculated across all spot estimates during the eight FOMC announcement days in 2022.

Table S4: Relative Discrepancies for Alternative Two-Candlestick Estimators

	VOO			Dollar/Yen		
	$p=1$	$p=2$	$p=4$	$p=1$	$p=2$	$p=4$
Panel A: Comparison versus the Stein-AMRE Estimator						
$\hat{\sigma}^p_{\text{Quad}}$	0.034	0.122	3.072	0.043	0.134	3.170
$(\hat{\sigma}^2_{\text{GK}})^{p/2}$	0.081	0.224	1.733	0.177	0.882	1.981
$(\hat{\sigma}_{\text{BLUE}})^p$	0.046	0.130	0.816	0.121	0.534	1.105
Panel B: Comparison versus the Quadratic-AMRE Estimator						
$\hat{\sigma}^p_{\text{Stein}}$	0.035	0.151	3.526	0.046	0.177	4.194
$(\hat{\sigma}^2_{\text{GK}})^{p/2}$	0.105	0.479	9.313	0.216	1.542	9.664
$(\hat{\sigma}_{\text{BLUE}})^p$	0.071	0.331	6.853	0.156	0.968	4.995

Note: The table reports summary statistics for the relative differences of alternative two-candlestick estimators of σ_t^p with respect to the AMRE estimators. In Panel A and Panel B, the benchmark AMRE estimators are set as $\hat{\sigma}^p_{\text{Stein}}(2)$ and $\hat{\sigma}^p_{\text{Quad}}(2)$, respectively. The reported values are the root mean squared relative differences, calculated across all spot estimates during the eight FOMC announcement days in 2022.

SC Monte Carlo Simulations

We evaluate the finite-sample performance of the proposed estimation methods through a Monte Carlo experiment. The data generating process for the price process is defined as follows

$$\begin{aligned} dP_t &= \sigma_t dW_t, \quad \sigma_t^2 = V_{1,t} + V_{2,t}, \\ dV_{1,t} &= 0.0128(0.4068 - V_{1,t})dt + 0.0954\sqrt{V_{1,t}}(\rho dW_t + \sqrt{1-\rho^2}dB_{1,t}), \\ dV_{2,t} &= 0.6930(0.4068 - V_{2,t})dt + 0.7023\sqrt{V_{2,t}}(\rho dW_t + \sqrt{1-\rho^2}dB_{2,t}), \end{aligned}$$

where W, B_1, and B_2 denote independent standard Brownian motions, $\rho = -0.7$, $V_{1,0} = V_{2,0} = 0.5$, so that $\sigma_0 = 1$. We simulate the "continuous-time processes" using a Euler scheme with mesh size being 10^{-4} minute. The candlesticks utilized in the calculations are constructed on 5-minute intervals, a common default choice in applied work, which we also adopt in our empirical study. The estimand σ_t^p with $p \in \{1, 2\}$ is sampled at a random point within each 5-minute estimation window. All numerical results reported below are based on 10,000 Monte Carlo replications.

To evaluate the potential distorting effects of market microstructure noise, we also consider a "noisy setting," in which the observed price, denoted by Y_t, is generated as

$$Y_t = P_t + \varepsilon_t,$$

where the ε_t noise terms are i.i.d. $\mathcal{N}(0, \varsigma^2)$. We examine values of $\varsigma \in \{5, 10, 20, 40, 80, 160\} \times 10^{-4}$. The value $\varsigma = 5 \times 10^{-4}$ is in line with the empirically realistic simulation settings of Da and Xiu (2021) and Li and Linton (2022). Hence, in addition to this "representative" noise level, our experiment also involves much larger noise levels to help illuminate the effect of sampling "too finely" relative to the magnitude of the noise.

Tables S5–S11 present the finite-sample biases, relative efficiencies under Stein's loss and the quadratic loss, and coverage rates of 90% confidence intervals (as detailed in footnote **??** of the main text) for various estimators. The finite-sample properties of these estimators under the no-noise scenario, displayed in Table S5, align with the asymptotic theory. The AMRE estimators exhibit the lowest risks, and the coverage rates for all confidence intervals are close to the nominal level.

As evidenced by Table S6, the results are effectively the same at an empirically realistic noise level of $\varsigma = 5 \times 10^{-4}$. This observation aligns with the "conventional wisdom" that in typical applications, microstructure noise has a negligible impact on volatility estimates based on a 5-minute sampling frequency.

Looking across Tables S7 to S11, the noise level is progressively doubled to highlight the potential distortion effects of noise. As the noise level increases, all estimators experience a growing

upward bias. The quadratic-AMRE estimator, $\hat{\sigma}^p_{\text{Quad}}$, is the only shrinkage estimator considered, and its inherent downward bias offers a unique advantage in counteracting the upward bias caused by the noise. When the noise level is not too high, the bias of the quadratic-AMRE estimator tends towards zero, and it eventually becomes the least biased estimator at very high noise levels. Consequently, $\hat{\sigma}^p_{\text{Quad}}$ achieves the lowest finite-sample quadratic risk across all the different settings. Furthermore, when the noise level is sufficiently high, $\hat{\sigma}^p_{\text{Quad}}$ surpasses $\hat{\sigma}^p_{\text{Stein}}$ and emerges as the minimum risk estimator in finite samples, even under Stein's loss.

Looking at the finite-sample coverage rates of the confidence intervals, it is interesting to note that as the noise level increases, the confidence intervals tend to cover the true value more frequently than the nominal level. This indicates that noise-induced distortion does not necessarily result in under-coverage. However, over-coverage is not consistently observed either. Indeed, at the highest noise level (Table S11), the confidence intervals all display severe under-coverage.

In summary, our simulation results support the widely-held belief that for empirically realistically calibrated noise levels, 5-minute coarse sampling effectively mitigates the detrimental impacts of the noise. Meanwhile, in more extreme situations with very high noise levels, the quadratic-AMRE estimator demonstrates superior finite-sample performance, primarily because its shrinkage properties allow it to partially counteract the upward bias induced by excessive noise.

Table S5: Finite-Sample Properties of Alternative Estimators: No Noise

	Spot Variance ($p = 2$)				Spot Volatility ($p = 1$)			
		Rel. Eff.				Rel. Eff.		
Estimator	Bias	Stein	Quad.	C.R.	Bias	Stein	Quad.	C.R.
$\hat{\sigma}^p_{\text{Stein}}$	-0.007	1.000	0.896	0.899	-0.005	1.000	0.975	0.899
$\hat{\sigma}^p_{\text{Quad}}$	-0.211	0.824	1.000	0.898	-0.063	0.937	1.000	0.899
$(\hat{\sigma}_{\text{BLUE}})^p$	0.050	0.984	0.841	0.898	-0.007	0.993	0.974	0.898
$(\hat{\sigma}^2_{\text{GK}})^{p/2}$	0.006	0.984	0.872	0.903	-0.029	0.971	0.981	0.902

Note: The table reports the finite-sample relative biases, relative efficiencies under Stein's and quadratic loss functions, and coverage rates of 90% confidence intervals for alternative estimators of the spot variance (left) and spot volatility (right). The noise level is set as $\varsigma = 0$.

Table S6: Finite-Sample Properties of Alternative Estimators: Noise Level $\varsigma = 5 \times 10^{-4}$

	Spot Variance ($p = 2$)				Spot Volatility ($p = 1$)			
		Rel. Eff.				Rel. Eff.		
Estimator	Bias	Stein	Quad.	C.R.	Bias	Stein	Quad.	C.R.
$\hat{\sigma}^p_{\text{Stein}}$	-0.004	1.000	0.887	0.903	0.001	1.000	0.969	0.902
$\hat{\sigma}^p_{\text{Quad}}$	-0.202	0.836	1.000	0.904	-0.057	0.944	1.000	0.903
$(\hat{\sigma}_{\text{BLUE}})^p$	0.062	0.980	0.832	0.903	-0.001	0.993	0.969	0.902
$(\hat{\sigma}^2_{\text{GK}})^{p/2}$	0.018	0.982	0.862	0.907	-0.023	0.974	0.979	0.906

Note: The table reports the finite-sample relative biases, relative efficiencies under Stein's and quadratic loss functions, and coverage rates of 90% confidence intervals for alternative estimators of the spot variance (left) and spot volatility (right). The noise level is set as $\varsigma = 5 \times 10^{-4}$.

Table S7: Finite-Sample Properties of Alternative Estimators: Noise Level $\varsigma = 1 \times 10^{-3}$

	Spot Variance ($p = 2$)				Spot Volatility ($p = 1$)			
		Rel. Eff.				Rel. Eff.		
Estimator	Bias	Stein	Quad.	C.R.	Bias	Stein	Quad.	C.R.
$\hat{\sigma}^p_{\text{Stein}}$	0.028	1.000	0.866	0.911	0.016	1.000	0.955	0.913
$\hat{\sigma}^p_{\text{Quad}}$	−0.182	0.864	1.000	0.913	−0.043	0.970	1.000	0.913
$(\hat{\sigma}_{\text{BLUE}})^p$	0.087	0.968	0.810	0.910	0.014	0.990	0.955	0.912
$(\hat{\sigma}^2_{\text{GK}})^{p/2}$	0.043	0.976	0.840	0.914	−0.008	0.983	0.970	0.915

Note: The table reports the finite-sample relative biases, relative efficiencies under Stein's and quadratic loss functions, and coverage rates of 90% confidence intervals for alternative estimators of the spot variance (left) and spot volatility (right). The noise level is set as $\varsigma = 1 \times 10^{-3}$.

Table S8: Finite-Sample Properties of Alternative Estimators: Noise Level $\varsigma = 2 \times 10^{-3}$

	Spot Variance ($p = 2$)				Spot Volatility ($p = 1$)			
		Rel. Eff.				Rel. Eff.		
Estimator	Bias	Stein	Quad.	C.R.	Bias	Stein	Quad.	C.R.
$\hat{\sigma}^p_{\text{Stein}}$	0.089	1.000	0.820	0.934	0.043	1.000	0.930	0.926
$\hat{\sigma}^p_{\text{Quad}}$	−0.134	0.949	1.000	0.935	−0.017	1.026	1.000	0.925
$(\hat{\sigma}_{\text{BLUE}})^p$	0.148	0.942	0.762	0.933	0.040	0.996	0.932	0.925
$(\hat{\sigma}^2_{\text{GK}})^{p/2}$	0.103	0.969	0.794	0.936	0.018	1.008	0.955	0.927

Note: The table reports the finite-sample relative biases, relative efficiencies under Stein's and quadratic loss functions, and coverage rates of 90% confidence intervals for alternative estimators of the spot variance (left) and spot volatility (right). The noise level is set as $\varsigma = 2 \times 10^{-3}$.

Table S9: Finite-Sample Properties of Alternative Estimators: Noise Level $\varsigma = 4 \times 10^{-3}$

	Spot Variance ($p = 2$)				Spot Volatility ($p = 1$)			
		Rel. Eff.				Rel. Eff.		
Estimator	Bias	Stein	Quad.	C.R.	Bias	Stein	Quad.	C.R.
$\hat{\sigma}^p_{\text{Stein}}$	0.244	1.000	0.730	0.962	0.119	1.000	0.873	0.935
$\hat{\sigma}^p_{\text{Quad}}$	−0.009	1.260	1.000	0.963	0.055	1.197	1.000	0.933
$(\hat{\sigma}_{\text{BLUE}})^p$	0.306	0.894	0.672	0.962	0.113	1.011	0.881	0.935
$(\hat{\sigma}^2_{\text{GK}})^{p/2}$	0.255	0.962	0.709	0.963	0.090	1.073	0.919	0.935

Note: The table reports the finite-sample relative biases, relative efficiencies under Stein's and quadratic loss functions, and coverage rates of 90% confidence intervals for alternative estimators of the spot variance (left) and spot volatility (right). The noise level is set as $\varsigma = 4 \times 10^{-3}$.

Table S10: Finite-Sample Properties of Alternative Estimators: Noise Level $\varsigma = 8 \times 10^{-3}$

	Spot Variance ($p = 2$)				Spot Volatility ($p = 1$)			
		Rel. Eff.				Rel. Eff.		
Estimator	Bias	Stein	Quad.	C.R.	Bias	Stein	Quad.	C.R.
$\hat{\sigma}^p_{\text{Stein}}$	0.633	1.000	0.660	0.935	0.289	1.000	0.836	0.865
$\hat{\sigma}^p_{\text{Quad}}$	0.302	1.926	1.000	0.936	0.216	1.377	1.000	0.860
$(\hat{\sigma}_{\text{BLUE}})^p$	0.703	0.883	0.612	0.942	0.279	1.041	0.855	0.871
$(\hat{\sigma}^2_{\text{GK}})^{p/2}$	0.631	0.986	0.651	0.937	0.249	1.168	0.909	0.868

Note: The table reports the finite-sample relative biases, relative efficiencies under Stein's and quadratic loss functions, and coverage rates of 90% confidence intervals for alternative estimators of the spot variance (left) and spot volatility (right). The noise level is set as $\varsigma = 8 \times 10^{-3}$.

Table S11: Finite-Sample Properties of Alternative Estimators: Noise Level $\varsigma = 1.6 \times 10^{-2}$

	Spot Variance ($p = 2$)				Spot Volatility ($p = 1$)			
		Rel. Eff.				Rel. Eff.		
Estimator	Bias	Stein	Quad.	C.R.	Bias	Stein	Quad.	C.R.
$\hat{\sigma}^p_{\text{Stein}}$	1.677	1.000	0.708	0.598	0.665	1.000	0.872	0.401
$\hat{\sigma}^p_{\text{Quad}}$	1.146	1.721	1.000	0.590	0.573	1.268	1.000	0.381
$(\hat{\sigma}_{\text{BLUE}})^p$	1.772	0.924	0.673	0.633	0.646	1.046	0.895	0.424
$(\hat{\sigma}^2_{\text{GK}})^{p/2}$	1.612	1.052	0.727	0.653	0.595	1.184	0.959	0.454

Note: The table reports the finite-sample relative biases, relative efficiencies under Stein's and quadratic loss functions, and coverage rates of 90% confidence intervals for alternative estimators of the spot variance (left) and spot volatility (right). The noise level is set as $\varsigma = 1.6 \times 10^{-2}$.

References

Da, R. and D. Xiu (2021): "When Moving-Average Models Meet High-Frequency Data: Uniform Inference on Volatility," *Econometrica*, 89, 2787–2825.

Li, J., D. Wang, and Q. Zhang (2022): "Reading the Candlesticks: An OK Estimator for Volatility," *Review of Economics and Statistics*, forthcoming.

Li, Z. M. and O. Linton (2022): "A ReMeDI for Microstructure Noise," *Econometrica*, 90, 367–389.

Olver, F. W., D. W. Lozier, R. F. Boisvert, and C. W. Clark (2010): *NIST Handbook of Mathematical Functions*, Cambridge University Press.